# A New Form of Decellularized Extracellular Matrix Hydrogel for Treating Ischemic Tissue via Intravascular Infusion

Martin T. Spang, Tori S. Lazerson, Saumya Bhatia, James Corbitt, Gerardo Sandoval, Colin Luo, Kent G. Osborn, Pedro Cabrales, Ester Kwon, Francisco Contijoch, Ryan R. Reeves, Anthony N. DeMaria, Karen L. Christman

University of California, San Diego

## Abstract

Extracellular matrix (ECM) hydrogels have been widely used in preclinical studies as injectable materials for tissue engineering therapies. We have developed a new ECM therapy, the soluble fraction derived from decellularized, digested ECM, for intravascular infusion. This new form of ECM is capable of gelation *in vivo* and can be delivered acutely after an injury to promote cell survival and improve vascularization. In this study, we show proof-of-concept for the feasibility, safety, and efficacy of ECM infusions using small and large animal models of acute myocardial infarction (MI) and intracoronary infusion. Following infusion, the ECM material was retained in the heart, specifically in regions of ischemia, and colocalized with endothelial cells, coating the leaky microvasculature. Functional improvements, specifically reduced left ventricular volumes, were observed after ECM infusion post-MI. Genes associated with angiogenesis were upregulated, and genes associated with cell apoptosis/necrosis and fibrosis were downregulated. The ECM was also delivered using a clinically-relevant catheter in a large animal model of acute MI. This study shows proof-of-concept for a new intravascular delivery strategy for ECM biomaterial therapies with potential implications for a variety of pathologies with ischemic tissue or injured vasculature.

Extracellular matrices (ECM) derived from decellularized tissues have shown promising results as tissue engineering scaffolds[1-4]. In particular, decellularized ECM can be processed via enzymatic digestion into inducible hydrogels that are capable of gelation at body temperature and can be injected for minimally-invasive procedures[5-8]. These hydrogels have a nanofibrous architecture reminiscent of native ECM, are degradable, and promote neovascularization, among a host of other pro-regenerative functions[2,9].

Current decellularized ECM biomaterials are limited to patches or injections. For most organs, patches require invasive surgeries for placement. Injections directly into tissue can be minimally invasive; however, they can cause localized trauma or organ perforation. Therefore, injections may not be feasible or could be delayed in certain clinical applications. Intravascular infusion is a potential alternative approach to ECM hydrogel injections, allowing for less invasive and potentially earlier delivery. An intravascular infusion during the acute time frame following injury could reduce cell death, promoting tissue salvage and maintenance. Furthermore, for ischemic injuries, intravascular infusion can take advantage of the leaky tissue vasculature that occurs acutely[10-13]. However, this delivery modality is not amenable to current ECM hydrogels because the liquid hydrogel contains not just soluble components, but also a translucent suspension of submicron particles that are too large to pass through leaky vasculature.

We aimed to develop a new form of decellularized ECM hydrogels that could be infused intravascularly, enabling delivery through the vasculature shortly following ischemic injuries. In the current study, we specifically developed a soluble version of a myocardial matrix hydrogel (SolMM) and evaluated intracoronary delivery as a treatment for acute myocardial infarction (MI). We previously developed the original myocardial matrix (MM) hydrogel, which is an ECM hydrogel derived from decellularized porcine myocardium, as a therapy for myocardial infarction. The MM hydrogel was shown to increase cardiac muscle and improve cardiac function in preclinical MI models[6-9]. A Phase I clinical trial was also completed with this material

using transendocardial injections in post-MI patients, which supported the safety and feasibility of this approach (ClinicalTrials.gov Identifier: NCT02305602)[14]. However, direct tissue injections in patients require delayed delivery because of acute risks related to ventricular rupture and arrythmias[3,15] while cardiomyocyte death and negative left ventricular (LV) remodeling are processes that commence within minutes to days after the MI. We initially hypothesized that intravascular infusion of SolMM would take advantage of the leaky vasculature following an acute ischemic injury permitting the biomaterial to pass through the vasculature and enter the ischemic region. We had previously shown that the original MM hydrogel reduced cardiomyocyte apoptosis and increased vascular density post-MI[9], suggesting the SolMM could improve myocardial salvage when delivered acutely and improve cardiac function. In terms of translation, intravascular infusion could easily be performed at the time of angioplasty using conventional techniques. In this study, we show development of a new form of ECM for intravascular infusion and proof-of-concept for its feasibility, safety, and efficacy using acute MI models.

## RESULTS

### Soluble extracellular matrix hydrogel can be isolated and is capable of gelation

The MM hydrogel was selected as a starting material for its demonstrated efficacy in preclinical models[6-9,18] and translational proof-of-concept in a Phase I clinical trial[14]. MM hydrogel was generated based on previously described protocols (Fig 1). In brief, fresh hearts were harvested from adult pigs, and the LV myocardium was isolated and minced (Fig 1a). Tissue was decellularized (Fig 1b), and the resulting ECM was lyophilized and milled into a fine powder (Fig 1c), followed by partial enzymatic digestion with pepsin. The material was then neutralized and buffered to match *in vivo* conditions, yielding the liquid MM hydrogel. While this material is

injectable, it is a translucent suspension (Fig 1d), which contains both soluble components and large submicron particulate, which would be too large to pass through leaky vasculature[19,20].

To generate an intravascularly infusible version of the ECM hydrogel, the MM hydrogel was centrifuged to separate the soluble and insoluble fractions (Fig 1e). The supernatant was isolated from the insoluble pellet, yielding the soluble MM fraction (SolMM). SolMM concentration was adjusted through dialysis and lyophilization, sterilized through filtration, lyophilized, and preserved at -80°C for long-term storage (Fig 1f, left). The SolMM was then resuspended in sterile water prior to injection (Fig 1f, right). We first demonstrated that this new form of ECM was still capable of gelation in tissue by subcutaneous injection in a rat (Fig 1g). Scanning electron microscope images of the subcutaneous gels demonstrated a nanofibrous architecture (Fig 1h) similar to most ECM hydrogels[21].

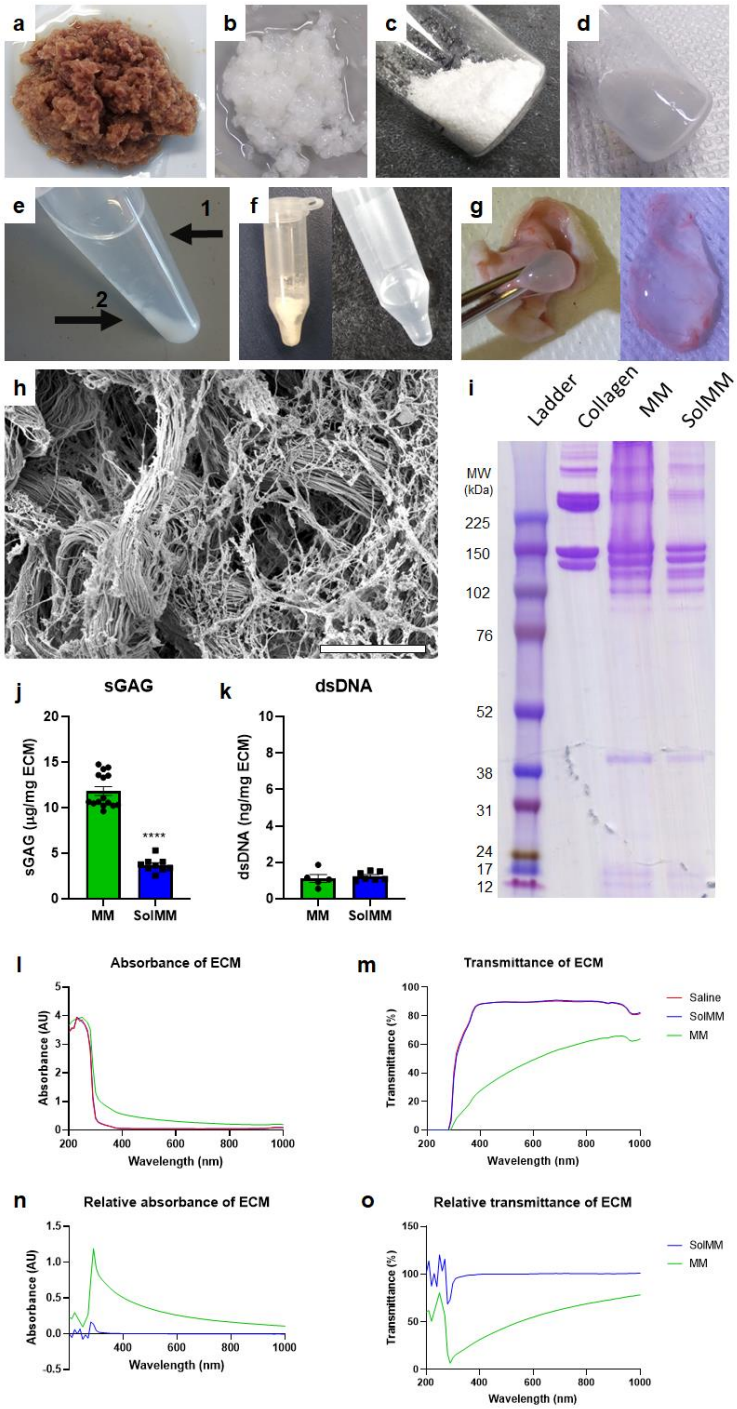


Figure 1: Generation and characterization of soluble myocardial matrix (SolMM). **a**, Isolated left ventricular myocardium is cut into pieces. **b**, Decellularized extracellular matrix (ECM) after continuous agitation in 1% sodium dodecyl sulfate. **c**, Lyophilized and milled ECM. **d**, Liquid myocardial matrix (MM) hydrogel. **e**, Fractionated MM after centrifugation; (1) SolMM fraction

supernatant and (2) insoluble pellet. **f**, Lyophilized (left) and resuspended (right) SolMM. **g**, Subcutaneous injection and gelation of SolMM. **h**, Scanning electron microscope image showing nanofibrous architecture of SolMM following gelation. Scale bar is 5 µm. **i**, Polyacrylamide gel electrophoresis of ladder, collagen, MM, and SolMM, showing that SolMM has decreased high molecular weight (150kDa+) proteins/peptides. **j**, Sulfated glycosaminoglycan (sGAG) content was significantly lower in SolMM vs MM. **k**, Double stranded DNA (dsDNA) content was not significantly different between SolMM and MM. **l-o**, Optical measurements of SolMM vs liquid MM. SolMM showed minimal differences in optical properties from saline whereas MM possessed increased absorbance and decreased transmittance. Absorbance sweep (**l**) and calculated transmittance (**m**) of SolMM, MM, and saline. **n**, Relative absorbance sweep (**n**) and relative calculated transmittance (**o**) of SolMM and MM.

Material characterization, including protein molecular weight distribution, double stranded DNA content (dsDNA), and sulfated glycosaminoglycan (sGAG) content, of the SolMM was compared to the original ECM hydrogel. As expected from the fractionation process, a decrease in intensity of high molecular weight proteins (>200 kDa) was observed (Fig 1i). SolMM possessed decreased sGAG content relative to the MM hydrogel, which was likely removed during the fractionating process (Fig 1j). dsDNA content, a marker of decellularization, was not significantly different between the full MM hydrogel and SolMM (Fig 1k).

Across most wavelengths tested, the optical properties of SolMM were nearly identical to saline. Relative to SolMM, the liquid MM showed an increase in absorbance and therefore a decreased transmittance (Fig 1l,m). When looking at relative absorbance and transmittance (accounting for the absorbance and transmittance of saline, Fig 1n,o), these results further reinforced the presence of large particles in liquid MM, and the absence of large particles in SolMM.

**Soluble extracellular matrix is hemocompatible**

As SolMM was derived from the MM hydrogel, it was expected that SolMM would be hemocompatible. While it is counterintuitive to think that decellularized ECM could be hemocompatible since exposed ECM initiates clotting *in vivo,* we previously demonstrated that the original MM hydrogel was hemocompatible, likely because of the digestion processing and low concentration[8]. SolMM was tested with human blood using the highest likely scenario of 1:1 SolMM to human blood and a physiologically relevant concentration of 1:10 SolMM, given the immediate dilution with blood following infusion. As shown in Figure 2, nearly all prothrombin times, red blood cell aggregation indices, as well as platelet aggregation with agonists fall within standard physiological ranges[22,23]. Additionally, fibrinogen and platelet concentrations were unaffected by the addition of SolMM (Fig 2d,e).

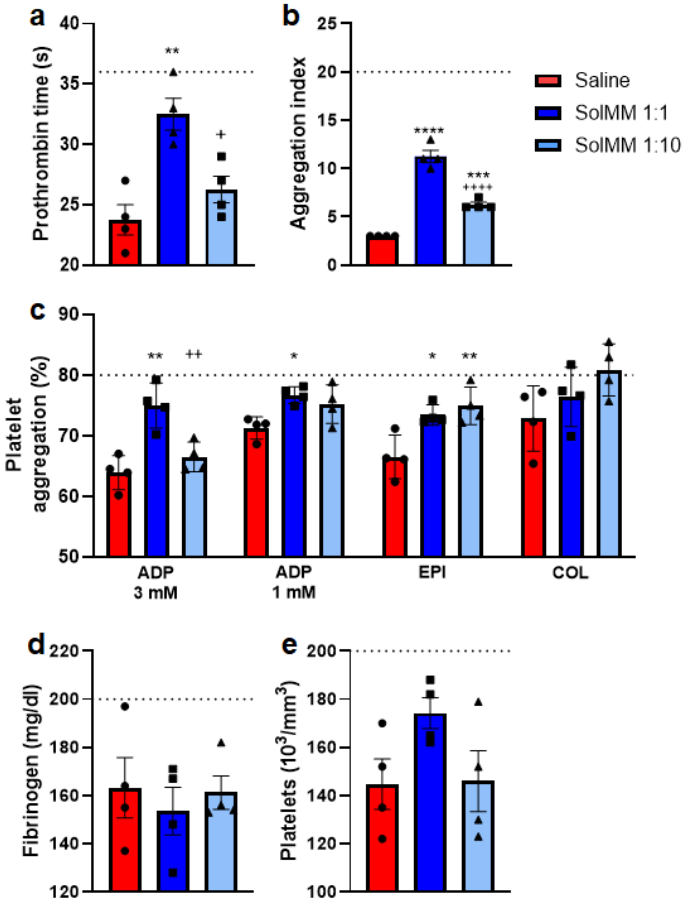


Figure 2: Hemocompatibility of soluble extracellular matrix (SolMM) with human blood and platelet rich plasma. **a**, Prothrombin time. **b**, Red blood cell aggregation index. **c**, platelet aggregation following addition of agonists: adenosine diphosphate (ADP), epinephrine (EPI), collagen (COL). Standard ranges for each parameter are indicated below dashed lines. SolMM does not affect the concentration of **e**, fibrinogen or **f**, platelets when mixed with human blood. N=4 human blood donors. * is relative to saline, and $^{+}$ is relative to 1:1 SolMM. Data are mean ± SEM.

**Soluble extracellular matrix infusions are localized to regions of ischemia**

Prior to infusions, SolMM was pre-labeled using an Alexa Fluor™ 568 conjugated N-hydroxysuccinimidyl ester that binds to free amines in SolMM. Simulated intracoronary infusions were performed in an ischemia-reperfusion rat model by injection of the material into the LV lumen during transient aortic clamping, which forces the material through the coronaries. After 30 min, 2, 6, 12, and 24 hours, hearts (n=2 per time point) were excised and evaluated via histology for material presence (Fig 3a), which was found to be localized to the infarcted region (Fig 3b,c). Minimal material was observed in the border zone (Fig 3d), and no material was seen in the remote myocardium (Fig 3e), including the septum and right ventricle. Material was distributed throughout the infarcted myocardium, suggesting tissue injury is required for material retention. To confirm this, SolMM infusions were performed in healthy rats without an MI as well in rats with a chronic MI wherein the material was infused 4 weeks post-MI. These rats did not show any matrix retention in the heart (Supplementary Figure 1); however, material was observed in the kidneys, suggesting almost immediate elimination through the kidneys. Red dye was also observed in the urine following animal euthanasia.

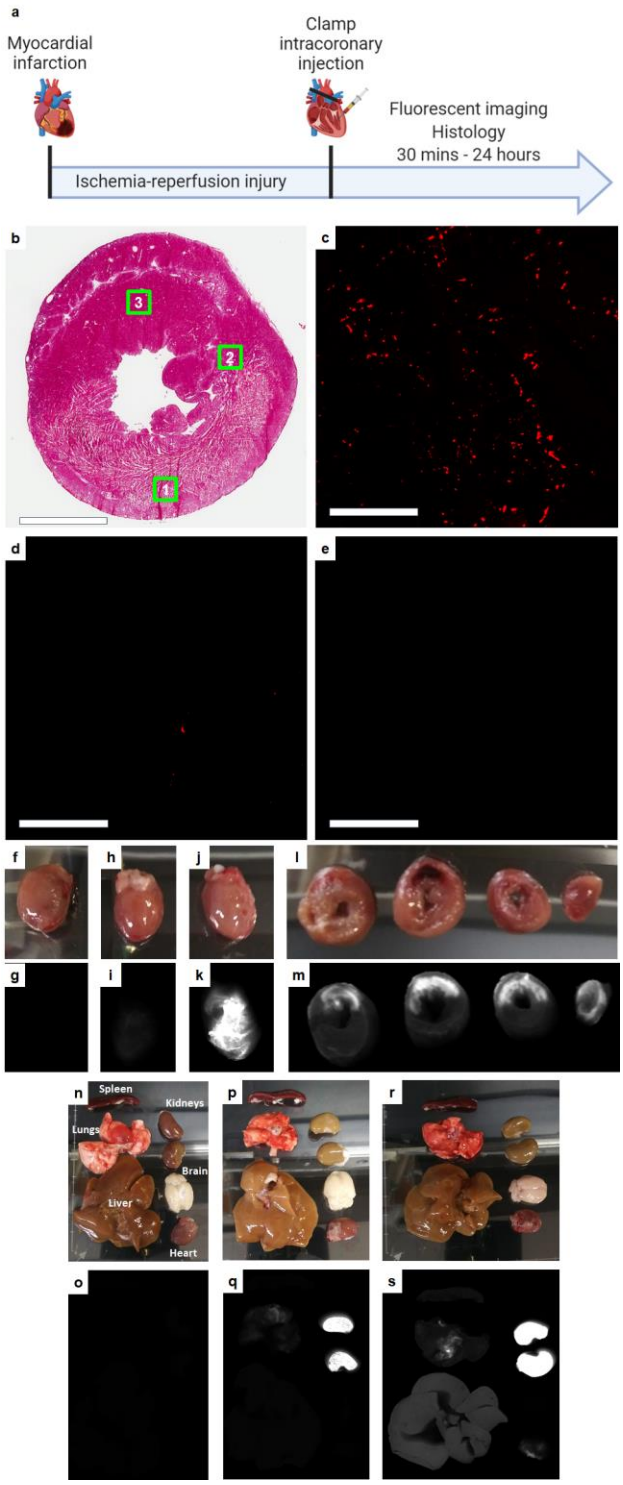


Figure 3: Soluble matrix (SolMM) infusions are localized to infarcted myocardium. **a**, Timeline of experiments. **b**, Hematoxylin & Eosin stain of short axis section of a representative heart following SolMM infusion, scale bar 3 mm. **c**-**e**, Red fluorescence images for locations shown in

insets in **b** of infarcted myocardium (**c**, 1), border zone (**d**, 2), and remote myocardium (**e**, 3), scale bars are 200 µm. **f**-**h**, Heart infrared scans 24 hours following MI procedure and infusion of saline without dye (**f**,**g**), trilysine conjugate with VivoTag®-S 750 (VT750, **h**,**i**), or SolMM conjugated with VT750 (**j**,**k**). **l**,**m**, Short axis slices of a SolMM infused heart from the base to the apex (left to right), infarct regions oriented in the upper portion of the slices. SolMM infused rats showed increased signal in the hearts, lungs and liver, with comparable signal in the kidneys as trilysine, suggesting rapid clearance. Organs are labeled in **n**, and the same orientation was used for **n**-**s**. Satellite organs (**n**,**p**,**r**), and corresponding near-infrared scans, VT750 in white (**o**,**q**,**s**). Harvested organs following MI and infusion of saline without VT750 (**n**,**o**), trylisine conjugated with VT750 (**p**,**q**), or SolMM conjugated with VT750 (**r**,**s**).

The pre-labeled material was tested at different doses, including 6, 10, and 12 mg/ml, (n=2 per dose) and showed a dose-dependent retention and distribution (Supplementary Figure 2). However, due to manufacturing limitations, specifically filtration, 10 mg/ml was the highest concentration that we could routinely produce. Retention of the 10 mg/ml material was assessed up to 7 days post-infusion to assess degradation. Material was retained up to approximately 3 days following infusion (Supplementary Figure 3).

To further verify delivery of the SolMM to infarcted myocardium, SolMM was conjugated with VivoTag®-S 750 (VT750) N-hydroxysuccinimidyl ester for visualization using an infrared imaging system. Using the same intracoronary infusion procedure following ischemia reperfusion in rats, controls animals were infused with saline (without dye) or trilysine conjugated with VT750. Unconjugated dye could bind to free amines in tissue, therefore, trilysine was conjugated with VT750 and served as a small non-gelling peptide control that should be cleared. Representative heart scans are shown in Figure 3f-k; saline infused (Fig. 3f,g) and dye labeled trilysine (Fig. 3h,i) infused hearts showed minimal signal relative to SolMM

infused hearts (Fig. 3j,k) 24 hours following infusion (n=3 per group). Figures 3k and 3m show localization to the infarct region in a SolMM infused heart that was sliced into multiple short axis sections. No signal or localization was observed in trilysine or saline infused heart short axis slices (Supplementary Figure 4). Satellite organs, including the lungs, liver, brain, kidney, and spleen, were also harvested and scanned (Fig 3n-s). Organ scans suggest that after passing through the heart, material accumulates in the liver and kidneys (Fig 3s).

**Soluble matrix shows co-localization with endothelial cells**

For safety evaluation, we wanted to confirm that SolMM was not blocking the lumen of blood vessels, starting from arterioles down to capillaries. We first stained for alpha-smooth muscle actin to label arterioles and confirmed that SolMM did not block arterioles (Fig 4a). We then stained for endothelial cells/capillaries using isolectin, which showed that the micron scale SolMM aggregates we observed were in fact overlapping with the microvasculature network (Fig 4b). Using confocal microscopy, z-stacks were obtained and suggested that material was present within the gaps between endothelial cells, resembling a fibrous matrix, and/or coating the inner lining, but not blocking the lumen of capillaries (Fig 4c-g).

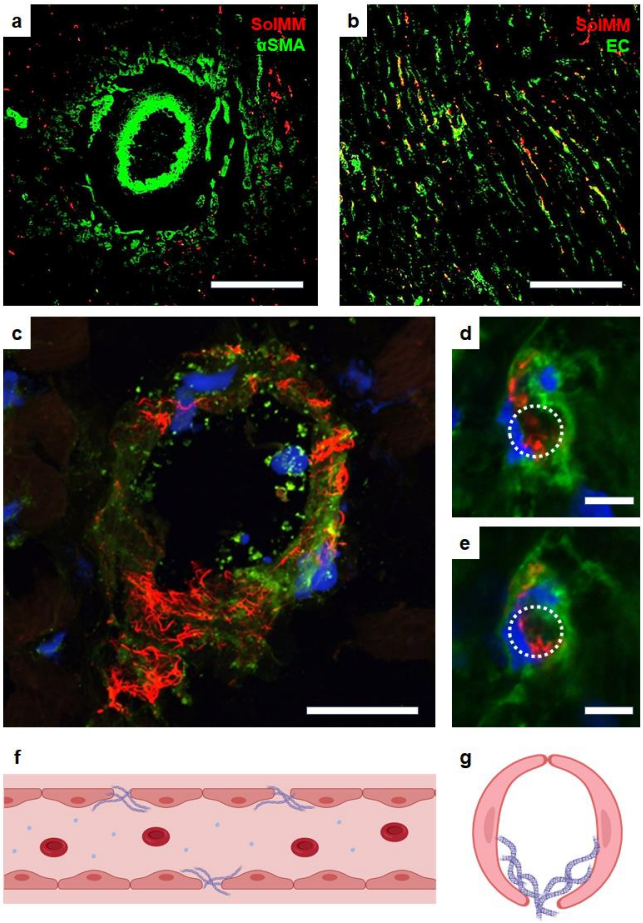


Figure 4: Staining for vasculature and soluble myocardial matrix (SolMM) localization post-myocardial infarction and infusion, showing colocalization of SolMM with the microvasculature as opposed to large vessels. SolMM was pre-labeled and visualized in red in **a**-**e**. **a**, Staining for arterioles using anti-alpha smooth muscle actin (αSMA) in green. (**b**-**e**), Staining for endothelial cells using isolectin in green. Scale bar is 200 µm for **a**,**b**. **c**, SolMM does not block the lumen of an arteriole, but appears to assemble and fill in the gaps in the endothelium. Scale bar is 25 µm. **d**,**e**, Representative sequential z-stack images of a capillary showing that SolMM coats the endothelial cells. Lumen traced with dotted white lines. Scale bar is 5 µm. **f**, Schematic diagram of longitudinal axis view of SolMM fibers assembling in the gaps in the endothelium in a leaky vessel. **g**, Schematic diagram of short axis view of SolMM coating a capillary.

**Soluble matrix infusion mitigates negative left ventricular remodeling**

To test the efficacy of SolMM infusions, rats (n=10-11 per group) underwent an MI, SolMM or saline infusion, and then magnetic resonance imaging (MRI) 24 hours and 5 weeks post-infusion (Fig 5a-c). At 24 hours following infusions, SolMM significantly decreased LV volumes, both end systolic (ESV, Fig 5d) and diastolic volumes (EDV, Fig 5e), compared to the saline control alongside a trending increase in ejection fraction (EF, Fig 5f). We confirmed that this was not a result of differences in infarct size between groups (Supplementary Fig. 5). This significant decrease in LV volumes of SolMM animals was maintained at 5 weeks post-infusion as well.

**Soluble matrix infusion increases vascularization and is pro-survival**

To determine how the SolMM improves cardiac function, hearts from animals that underwent MRI were harvested and were stained for vessels. Two additional sets of hearts were harvested 1 and 3 days post-MI and infusion for histological and gene expression analyses (Fig 5j). These time points were selected based on the observed functional improvements at 24 hours (Fig 5b-f) and the degradation time of SolMM, as it is retained up to approximately 3 days post-infusion (Supplementary Figure 3). RNA was isolated from the LV free wall of hearts 1 and 3 days post-infusion. Genes were selected from a previous time course study of the LV transcriptome up to 48 hours post-MI[24]. Additionally, genes were selected from a microarray study of the effects of full MM hydrogel in a sub-acute model of MI[9].

As the full MM hydrogel was previously shown to increase vascularization and be pro-survival[9,25], we hypothesized that SolMM infusions would likewise increase vascularization and reduce cardiomyocyte apoptosis. At 5 weeks post-infusion, SolMM significantly increased infarct vascularization over saline infused controls (Fig 5g-i). At 3 days post-infusion, SolMM significantly decreased the number of cardiomyocytes undergoing apoptosis in the border zone

region (Fig 5k-m). qRT-PCR further confirmed these pathways with a trending increase in angiopoietin (ANGPT2) expression alongside a significant increase in placental growth factor (PGF) expression (Fig 5n) one day after infusion, suggesting early upregulation of angiogenic pathways. A trending decrease was observed in caspase 3 (CASP3) expression and growth arrest and DNA damage inducible gamma (GADD45G) expression, suggesting decreased apoptosis/necrosis pathways (Fig 5o).

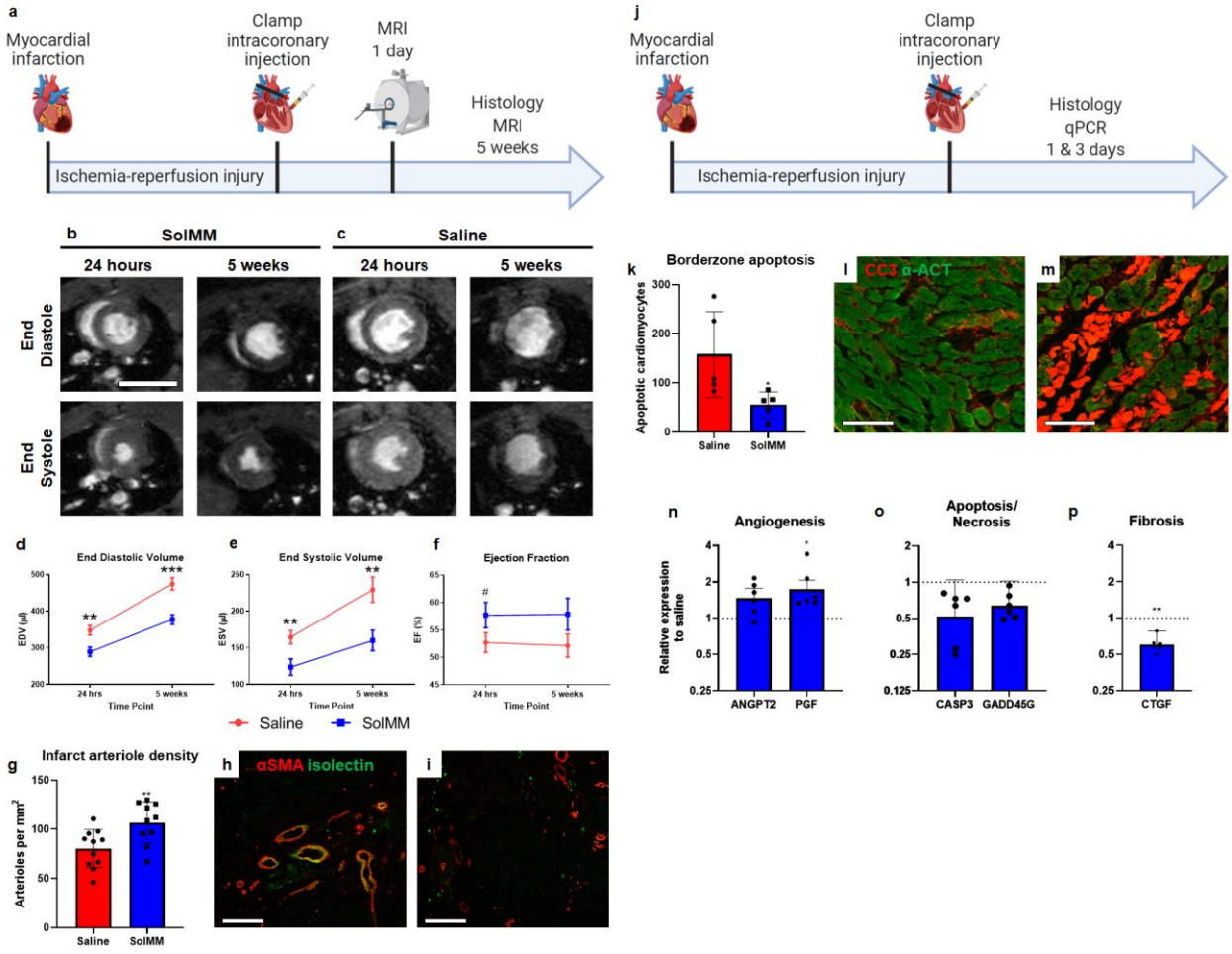


Figure 5: Soluble matrix (SolMM) infusions significantly improve cardiac function post-MI. **a**, Timeline of efficacy study. **b**-**c**, Representative magnetic resonance images at 24 hours and 5 weeks post-injection of SolMM (**b**) or saline (**c**). Scale bar 10 mm. **d**-**f**, SolMM infusions

preserve left ventricle volumes at 24 hours and 5 weeks post-MI; end diastolic volume (**d**, EDV), end systolic volume (**e**, ESV), ejection fraction (**f**, EF). **g**, Infarct arteriole density increased with SolMM infusions at 5 weeks post-infusion, promoting neovascularization. Representative images of SolMM (**h**) and saline (**i**) infused hearts; alpha smooth muscle actin (αSMA) in red for arterioles and isolectin in green for endothelial cells. Scale bar 250 µm. **j**, Timeline of acute mechanisms of repair study. Mechanisms of repair were evaluated through histology (**k**-**m**) and gene expression (**n**-**p**) analyses. **k**, Number of cardiomyocytes undergoing apoptosis significantly decreased in the border zone of SolMM infused hearts at 3 days post-infusion. Representative images of SolMM (**i**) and saline (**m**) infused hearts; cleaved caspase 3 (CC3) for apoptosis in red and alpha actinin (α-ACT) for cardiomyocytes in green. Scale bar 100 µm. **n**-**p**, Gene expression analysis at acute timepoints (angiogenesis at 1 day; apoptosis/necrosis and fibrosis at 3 days). Angiopoietin (ANGPT2), placental growth factor (PGF), caspase 3 (CASP3), growth arrest and DNA damage inducible gamma (GADD45G), connective tissue growth factor (CTGF). Data are mean ± SEM.

The full MM hydrogel was also previously shown to decrease infarct and interstitial fibrosis[8,9] and therefore we evaluated both indices at 5 weeks SolMM infusion. However, infarct fibrosis and interstitial fibrosis were not significantly different between groups (Supplemental Figure 5), but a fibrotic pathway was shown to be differentially expressed at 3 days post-infusion (Fig 5p), specifically a significant decrease in connective tissue growth factor (CTGF) expression.

**Soluble extracellular matrix is capable of intravascular infusion using a clinically-relevant catheter**

Given the promising results in small animal acute MI models, we wanted to perform a pilot in a large animal model to establish whether SolMM delivery via infusion could also be achieved using a clinically-relevant infusion catheter. To ensure that SolMM would pass through a catheter, pre-gel complex viscosity was measured relative to saline and full liquid MM (Fig 6a). The pre-gel complex viscosity of SolMM was an order of magnitude lower than MM, but still higher than saline. Despite the increased viscosity, SolMM was able to pass through a catheter with an internal diameter of 0.36 mm. In Yucatan minipigs, an MI was induced by inflating a balloon in the left anterior descending (LAD) artery for 90 min, followed by reperfusion, simulating a balloon angioplasty (Fig 6b). The same balloon was then used for fluorescently tagged SolMM or trilysine infusion (n=2 each group) 30 minutes after reperfusion.

As seen in the small animal model, SolMM was observed in the infarct region in the porcine MI model (Figs 6c,d). Likewise, SolMM was distributed throughout the infarcted myocardium and was not observed in the border zone or remote myocardium (Supplementary Figure 6). Satellite organs, including lungs, liver, brain, kidneys, and spleen, were harvested and did not show any signs of material, ischemia, or inflammation (Supplementary Figure 7, Supplementary Table 1). SolMM was observed to similarly line endothelial cells of the infarcted myocardium in the pig model (Fig 6e,f ). In contrast, no signal was observed in the infarct region with the trilysine control (Supplementary Figure 6).

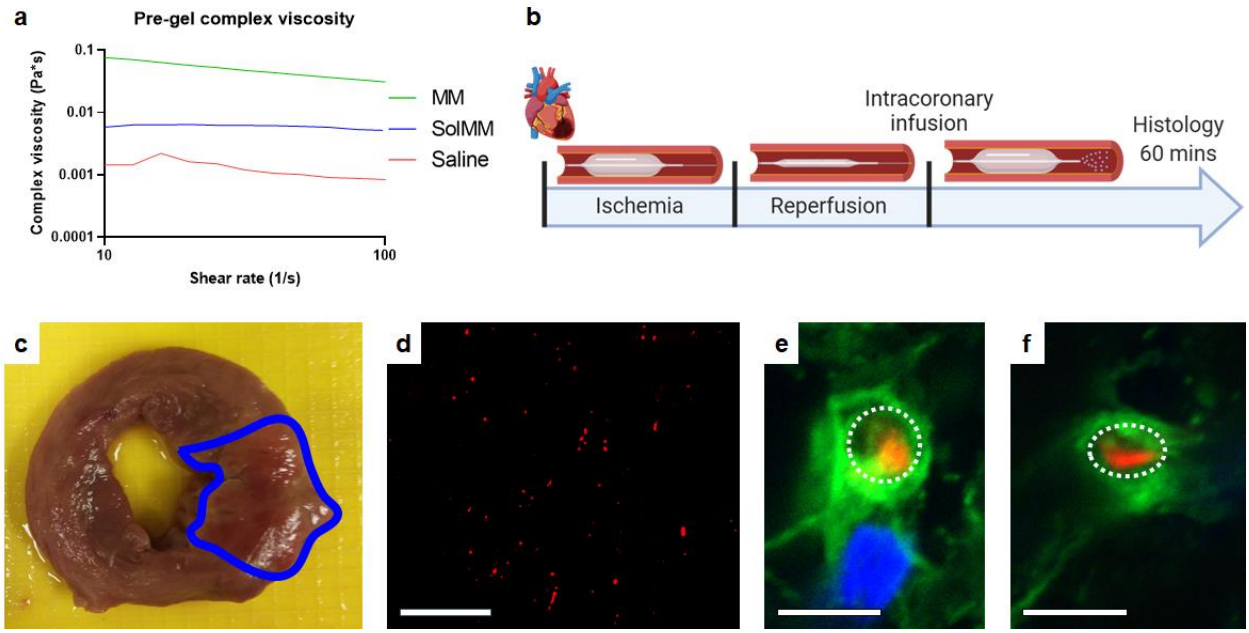


Figure 6: Soluble matrix (SolMM) infusions are amenable to intracoronary infusion with a balloon infusion catheter. **a**, SolMM pre-gel complex viscosity is lower than its full matrix (MM) counterpart, suggesting potential for catheter delivery. **b**, Timeline of catheter feasibility study. **c**, Macroscopic short-axis view of a pig heart post-MI and SolMM infusion. Infarct outlined in blue. **d**, Fluorescent image of SolMM (red) distribution and retention in a histological section from the same heart. Scale bar 200 µm. **e**,**f**, Representative confocal images of SolMM (red) and endothelial cells (green) from SolMM infused pigs. SolMM lines the endothelial cells of infarcted myocardium, as similarly observed in the rat MI model. Lumen traced with dotted white lines Scale bars 5 µm.

## Discussion

In this study, we developed a new form of decellularized ECM, an intravascularly infusible ECM hydrogel. Similar to our previous full version of the MM hydrogel, the SolMM was hemocompatible and we found no evidence of embolization, showing the material can be safely

delivered intravascularly. Our initial hypothesis was that SolMM would pass through the leaky vasculature through the gaps in the endothelial cell layer and into the tissue as was previously seen with an infusible alginate material in a pre-clinical porcine MI model[11]. Instead, we found that the soluble ECM hydrogel coats and/or fills in the gaps between endothelial cells (Fig 4), specifically endothelial cells in the infarcted region of the heart. It is known that there are numerous changes to the endothelium during acute ischemia, including upregulation of integrins and other receptors as well as pre-existing integrins undergoing functional changes, which cause their release from the underlying ECM and formation of clusters on the cell membrane[26,27]. These changes may result in the ability of the endothelial cells at locations of acute ischemia to bind the SolMM. Notably, the trilysine peptide control did not bind, suggesting there may be specific receptor-ligand interactions with the SolMM.

Even though the SolMM and full MM hydrogel are derived from the same tissue source, there are key differences. Unlike the full ECM hydrogel, which forms larger boluses upon direct injection, the SolMM is distributed into micron-scale regions, which can be degraded more quickly because of their small size. The observed degradation time of SolMM at 3 days is significantly shorter than the full MM hydrogel, which degrades over approximately 3 weeks[8]. Due to the diffuse nature of SolMM following its delivery, it could be more appropriate to compare SolMM to peptide therapeutics as opposed to other ECM hydrogel therapies. This comparison to peptides is evident in the clearance of non-retained SolMM, which like other peptide therapeutics[28,29] appears to be rapidly excreted by the kidneys since we observed labelled material in the urine of rats and in the kidneys shortly following infusion (Fig 3s). Additionally, peptide therapeutics are prone to proteolysis in the blood, liver, and kidneys. The material was not observed in the kidneys in the pig model; however, this was likely due to the detection limit of histology. SolMM has advantages over traditional peptide therapeutics due to increased retention through potential binding and gelation in the heart as we observed the

appearance of a fibrous matrix in the microvasculature (Fig. 4c). This could shield the material from proteolysis, allowing for increased tissue retention and therapeutic effects, as opposed to relying on systemic delivery and passive diffusion through capillaries[29]. In terms of efficacy, SolMM significantly reduced both end-diastolic and end-systolic volumes one day after MI and infusion compared to saline. This difference was maintained, but did not further improve out to 5 weeks post-infusion (Fig 5d,e). This is in line with the observed degradation time of SolMM, approximately 3 days, where there is an initial therapeutic effect. Additionally, fibrotic pathways were differentially expressed shortly after SolMM infusion, specifically CTGF whose overexpression has been implicated in cardiac fibrosis[30]. The opposite trend was observed in SolMM infused hearts acutely post-infusion, suggesting that SolMM mitigates fibrosis. However, it is likely that the therapeutic effect of SolMM is decreased after degradation, and then fibrotic pathways resume as we found no significant differences in fibrosis at 5 weeks post infusion. This is in contrast to the full MM hydrogel, which was capable of reducing fibrosis post-intramyocardial injection[8,9].

ECM hydrogels have been shown to create a pro-remodeling over a pro-inflammatory environment, leading to increases in vascularization and cell survival[6,9,31]. We hypothesized SolMM delivered acutely after an MI would lead to increased cardiomyocyte survival and infarct vascularization through similar mechanisms as the full MM hydrogel. Indeed, we found decreased numbers of apoptotic cardiomyocytes and increased arteriole density with the SolMM. However, based on the observation that SolMM coats endothelial cells as opposed to entering the tissue, the mechanisms leading to improved survival and vascularization may be different between the SolMM and full MM hydrogel. As the SolMM directly interfaces with endothelial cells, the early therapeutic effects we observed could be related to improvements in endothelial cell function and cell survival, shielding from reperfusion injury, or modulation of the acute inflammatory response.

We have demonstrated proof-of-concept for the feasibility, safety, and efficacy of an ECM hydrogel for intravascular infusion in rat acute MI model. Therapeutic effects were observed early and maintained, creating a better baseline, which could have clinical implications. In addition, we showed that SolMM was able to be delivered with a balloon infusion catheter and retained within the microvasculature in a porcine MI model, demonstrating potential clinical relevance. The material was only observed in the infarcted tissue, as also seen in the small animal model, demonstrating that the endothelial cell injury and SolMM retention is conserved across species. There are, however, several studies that will need to be performed prior to translation, including dose optimization, efficacy in a large animal, and further safety studies to evaluate any off-target effects.

ECM infusions are a versatile new platform for the regenerative medicine and tissue engineering field. In this study, we chose to focus on the cardiac application of ECM infusions; however, soluble ECM could be generated from any type of decellularized tissue, and ECM infusions could be applied to many diseases or injuries where there is endothelial cell injury or dysfunction. Whereas traditional tissue engineering approaches have focused on scaffolds and/or cells to replace/repair damaged tissue, infusible ECM therapies could shift the focus towards treating the microvasculature to improve tissue function.

**Acknowledgements**

Funding was provided by the NIH NHLBI (R01HL113468). MTS was supported by NIH NHLBI T32HL105373 and AHA pre-doctoral fellowship. The authors would like to thank Jesse Placone for his confocal imaging assistance, Ray Wang and Pamela Duran for their helpful comments during the manuscript editing process, and the University of California, San Diego Institutional Animal Care and Use Program animal health technicians for large animal anesthesia assistance.

**Author contributions**

KLC obtained the funding. MTS, KLC, RRR, and AND conceptually designed the studies. MTS, KLC, and AND interpreted the results. CL performed small animal surgeries and assisted with large animal studies. RRR performed large animal surgeries. KGO performed large animal necropsy and histopathology analysis. MTS, TSL, SB, JC, and GS processed tissue samples and performed analyses. PC designed and performed hemocompatibility analysis. EW and FC provided consultation, experimental design, and data evaluation related to imaging analysis. MTS and KLC drafted the manuscript. All authors edited the manuscript.

**Competing interests**

KLC and AND hold equity in Ventrix, Inc. KLC is a co-founder, consultant, board member, and receives income from Ventrix, Inc.

**Additional information**

Supplementary information is available for this paper online.

Correspondence and requests for materials should be addressed to KLC.

References


1. Badylak, S.F. The extracellular matrix as a biologic scaffold material. *Biomaterials* **28**, 3587-3593 (2007).
2. Saldin, L.T., Cramer, M.C., Velankar, S.S., White, L.J. & Badylak, S.F. Extracellular matrix hydrogels from decellularized tissues: Structure and function. *Acta Biomaterialia* **49**, 1-15 (2017).
3. Spang, M.T. & Christman, K.L. Extracellular matrix hydrogel therapies: In vivo applications and development. *Acta Biomaterialia* **68**, 1-14 (2018).
4. Badylak, S.F., Freytes, D.O. & Gilbert, T.W. Extracellular matrix as a biological scaffold material: Structure and function. Vol. 5 1-13 (2009).
5. Freytes, D.O., Martin, J., Velankar, S.S., Lee, A.S. & Badylak, S.F. Preparation and rheological characterization of a gel form of the porcine urinary bladder matrix. *Biomaterials* **29**, 1630-1637 (2008).
6. Singelyn, J.M.*, et al.* Naturally derived myocardial matrix as an injectable scaffold for cardiac tissue engineering. *Biomaterials* **30**, 5409-5416 (2009).
7. Singelyn, J.M.*, et al.* Catheter-deliverable hydrogel derived from decellularized ventricular extracellular matrix increases endogenous cardiomyocytes and preserves cardiac function post-myocardial infarction. *Journal of the American College of Cardiology* **59**, 751-763 (2012).
8. Seif-Naraghi, S.B.*, et al.* Safety and efficacy of an injectable extracellular matrix hydrogel for treating myocardial infarction. *Science translational medicine* **5**, 173ra125-173ra125 (2013).
9. Wassenaar, J.W.*, et al.* Evidence for Mechanisms Underlying the Functional Benefits of a Myocardial Matrix Hydrogel for Post-MI Treatment. *Journal of the American College of Cardiology* **67**, 1074-1086 (2016).

10. Nguyen, M.M.*, et al.* Enzyme-Responsive Nanoparticles for Targeted Accumulation and Prolonged Retention in Heart Tissue after Myocardial Infarction. *Advanced Materials* **27**, 5547-5552 (2015).

11. Leor, J.*, et al.* Intracoronary Injection of In Situ Forming Alginate Hydrogel Reverses Left Ventricular Remodeling After Myocardial Infarction in Swine. *Journal of the American College of Cardiology* **54**, 1014-1023 (2009).

12. Cao, R.*, et al.* Comparative evaluation of FGF-2-, VEGF-A-, and VEGF-C-induced angiogenesis, lymphangiogenesis, vascular fenestrations, and permeability. *Circulation research* **94**, 664-670 (2004).

13. Weis, S.*, et al.* Src blockade stabilizes a Flk/cadherin complex, reducing edema and tissue injury following myocardial infarction. *Journal of Clinical Investigation* **113**, 885-894 (2004).

14. Traverse, J.H.*, et al.* First-in-Man Study of a Cardiac Extracellular Matrix Hydrogel in Early and Late Myocardial Infarction Patients. *JACC: Basic to Translational Science* (2019).

15. Johnson, T.D. & Christman, K.L. Injectable hydrogel therapies and their delivery strategies for treating myocardial infarction. *Expert opinion on drug delivery* **10**, 59-72 (2013).

16. Frey, N.*, et al.* Intracoronary delivery of injectable bioabsorbable scaffold (IK-5001) to treat left ventricular remodeling after ST-elevation myocardial infarction: A first-in-man study. *Circulation: Cardiovascular Interventions* **7**, 806-812 (2014).

17. Rao, S.V.*, et al.* Bioabsorbable Intracoronary Matrix for Prevention of Ventricular Remodeling After Myocardial Infarction. *Journal of the American College of Cardiology* **68**, 715-723 (2016).

18. Wang, R.M. & Christman, K.L. Decellularized myocardial matrix hydrogels: In basic research and preclinical studies. *Advanced Drug Delivery Reviews* **96**, 77-82 (2016).

19. Hobbs, S.K.*, et al.* Regulation of transport pathways in tumor vessels: Role of tumor type and microenvironment. *Proceedings of the National Academy of Sciences of the United States of America* **95**, 4607-4612 (1998).

20. Alexis, F., Pridgen, E., Molnar, L.K. & Farokhzad, O.C. Factors affecting the clearance and biodistribution of polymeric nanoparticles. Vol. 5 505-515.

21. Ungerleider, J.L., Johnson, T.D., Rao, N. & Christman, K.L. Fabrication and characterization of injectable hydrogels derived from decellularized skeletal and cardiac muscle. *Methods (San Diego, Calif.)* **84**, 53-59 (2015).

22. White, M.M. & Jennings, L.K. *Platelet Protocols: Research and Clinical Laboratory Procedures*, (1999).

23. Vayá, A.*, et al.* Erythrocyte aggregation determined with the Myrenne aggregometer at two modes (M0, M1) and at two times (5 and 10 sec). Vol. 29 119-127 (2003).

24. Harpster, M.H.*, et al.* Earliest changes in the left ventricular transcriptome postmyocardial infarction. *Mammalian Genome* **17**, 701-715 (2006).

25. Gaetani, R.*, et al.* Cardiac-Derived Extracellular Matrix Enhances Cardiogenic Properties of Human Cardiac Progenitor Cells. *Cell Transplantation* **25**, 1653-1663 (2016).

26. Tagaya, M.*, et al.* Rapid loss of microvascular integrin expression during focal brain ischemia reflects neuron injury. *Journal of cerebral blood flow and metabolism : official journal of the International Society of Cerebral Blood Flow and Metabolism* **21**, 835-846 (2001).

27. Stupack, D.G. & Cheresh, D.A. Integrins and Angiogenesis. *Current Topics in Developmental Biology* **64**, 207-238 (2004).

28. Fosgerau, K. & Hoffmann, T. Peptide therapeutics: current status and future directions. *Drug Discovery Today* **20**(2015).

29. Di, L. Strategic Approaches to Optimizing Peptide ADME Properties. *AAPS Journal* **17**, 134-143 (2015).

30. Chen, M.M., Lam, A., Abraham, J.A., Schreiner, G.F. & Joly, A.H. CTGF expression is induced by TGF- beta in cardiac fibroblasts and cardiac myocytes: a potential role in heart fibrosis. *Journal of molecular and cellular cardiology* **32**, 1805-1819 (2000).

31. Ungerleider, J.L.*, et al.* Extracellular Matrix Hydrogel Promotes Tissue Remodeling, Arteriogenesis, and Perfusion in a Rat Hindlimb Ischemia Model. *JACC: Basic to Translational Science* **1**(2016).

32. Syedain, Z.H.*, et al.* A completely biological "off-the-shelf" arteriovenous graft that recellularizes in baboons. *Science Translational Medicine* **9**(2017).

33. Oronsky, B., Oronsky, N. & Cabrales, P. Platelet inhibitory effects of the phase 3 anticancer and normal tissue cytoprotective agent, RRx-001. *Journal of Cellular and Molecular Medicine* **22**, 5076-5082 (2018).

34. Jani, V.P., Yalcin, O., Williams, A.T., Popovsky, M.A. & Cabrales, P. Rat red blood cell storage lesions in various additive solutions. *Clinical Hemorheology and Microcirculation* **67**, 45-57 (2017).

35. Buono, M.J., Krippes, T., Kolkhorst, F.W., Williams, A.T. & Cabrales, P. Increases in core temperature counterbalance effects of haemoconcentration on blood viscosity during prolonged exercise in the heat. *Experimental Physiology* **101**, 332-342 (2016).

36. Bonios, M.*, et al.* Myocardial substrate and route of administration determine acute cardiac retention and lung biodistribution of cardiosphere-derived cells. *Journal of Nuclear Cardiology* **18**, 443-450 (2011).

37. Cheng, K.*, et al.* Magnetic enhancement of cell retention, engraftment, and functional benefit after intracoronary delivery of cardiac-derived stem cells in a rat model of ischemia/reperfusion. *Cell transplantation* **21**, 1121-1135 (2012).

38. Wassenaar, J.W., Braden, R.L., Osborn, K.G. & Christman, K.L. Modulating in vivo degradation rate of injectable extracellular matrix hydrogels. *J. Mater. Chem. B* **4**, 2794-2802 (2016).

39. Ren, Y., *et al.* Targeted tumor-penetrating siRNA nanocomplexes for credentialing the ovarian cancer oncogene ID4. *Science Translational Medicine* **4**(2012).

40. Freyman, T., *et al.* A quantitative, randomized study evaluating three methods of mesenchymal stem cell delivery following myocardial infarction. *European Heart Journal* **27**, 1114-1122 (2006).